RSC Advances

ROYAL SOCIETY OF CHEMISTRY

www.rsc.org/advances

exposure

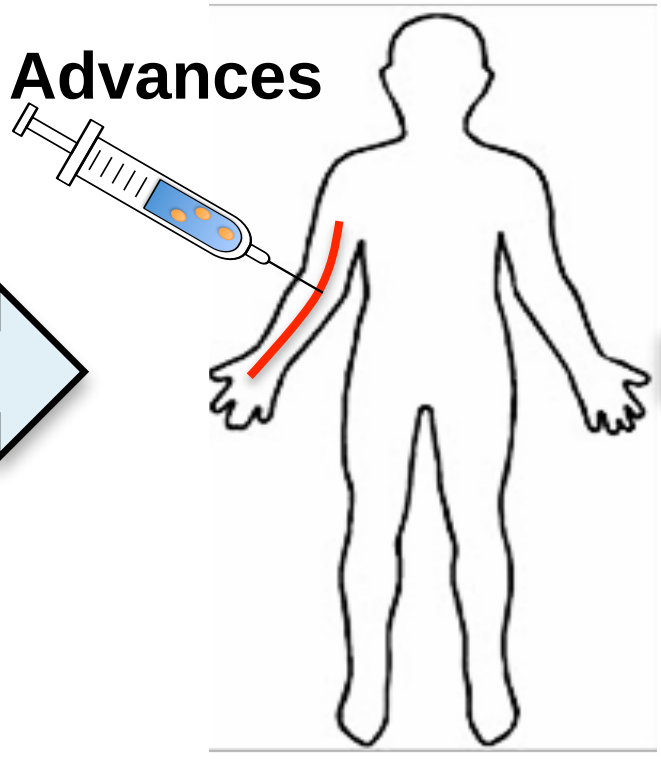

corona formation

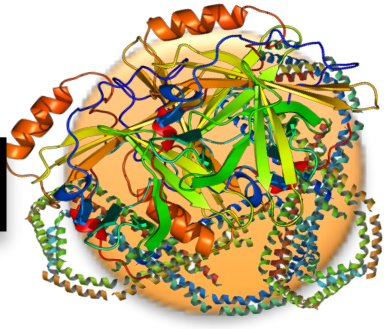

targeting

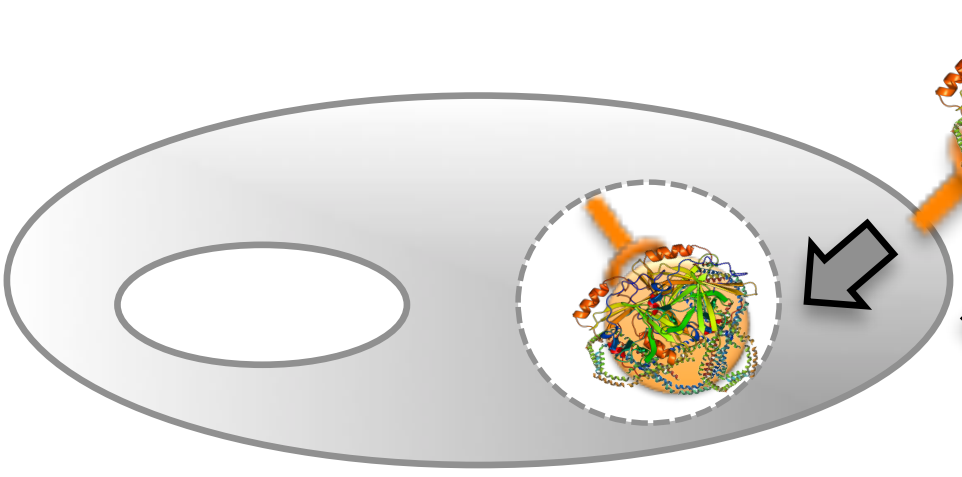

1. Synthetic identity

2. Biological identity

3. Physiological response

Journal Name

RSCPublishing

ARTICLE

Lipid composition: A "key factor" for the rational manipulation of the liposome-protein corona by liposome design

Cite this: DOI: 10.1039/x0xx00000x

Received 00th January 2012,
Accepted 00th January 2012

DOI: 10.1039/x0xx00000x

www.rsc.org/

G. Caracciolo,*[a] D. Pozzi,[a] A. L. Capriotti,[b] C. Cavaliere,[b] S. Piovesana,[b] H. Amenitsch,[c] and A. Laganà[b]

When liposomes are exposed to biological fluids, a dynamic coating of proteins immediately covers them. Similarly to the aura of plasma surrounding the Sun, plasma proteins are thought of as establishing an aura that surrounds each liposome, hence the phenomenon was dubbed 'protein corona'. This natural functionalization includes proteins engaged from the blood that can interact with receptors (over)expressed on the plasma membrane of target cells, thus targeting the liposomes to their final destination. Exploiting the liposome-protein corona for targeting has the potential to revolutionize the treatment of many disorders and requires a deep understanding of the factors shaping the corona. Following incubation with human plasma (HP), here we manipulated this corona by using six liposomal formulations with systematic changes in lipid composition. The lipids we employed are among the most frequently used lipid species for drug and gene delivery applications in vitro and in vivo. The six liposome-protein coronas were thoroughly characterized by synchrotron small angle X-ray scattering, dynamic light scattering, zeta-potential and nanoliquid-cromatography tandem mass spectrometry experiments. We identified general principles shaping the liposome-protein corona and established clear-cut relationships between lipid species and classes of plasma proteins. This knowledge sets the basis for a rational manipulation of the protein corona for targeted drug delivery by liposome design.

Introduction

Liposomes – closed bilayer vesicles made up of phospholipids containing an aqueous core – are considered to be the best class of organic nanoparticles for the treatment of many diseases.[1, 2] Liposomes can carry hydrophilic or hydrophobic payloads embedded either in the interior core or in the lipid bilayer. Due to controllable synthetic identity (size, charge and surface chemistry), liposomes have emerged as a robust delivery platform. As a proof, one can consider that the majority of currently approved marketed nanomedicines are liposome-based formulations.[3] As drug delivery systems liposomes attracted a lot of attention after Doxil® was approved by the Food and Drug Administration (FDA) as a treatment for AIDS-related Kaposi's sarcoma.[4] Nowadays, widespread application of liposomal nanomedicine is greatly impeded by limited understanding and control over their bio-nano-interactions with biological systems. When liposomes enter in contact with a biological fluid (e.g. the blood), proteins compete for space on the liposome surface forming what is referred to as the 'protein corona'.[5-16] The structure, thickness, surface charge and composition of the corona depend on the physical-chemical features of the liposome and the length of exposure.[17-19] The resulting biological identity can drastically differ from its original synthetic one (Figure 1) and is related to relevant biological processes such as immune response, complement activation, coagulation and thrombosis. Recent findings show that the protein corona is also formed on PEGylated liposomes, but is slightly thinner.[20] As corona formation on liposomes in vivo is not completely avoidable, it has been conceived that these tightly associated proteins can play a pivotal role in the bio-nano-interactions as they will determine the interface "seen" and "read" by the living organism.[9, 10] With this notion, the liposome-protein corona is transformed from a problem to an opportunity.[21, 22] The adsorbed protein layer or corona will include proteins that could target the liposome to specific plasma membrane receptors. If the corona composition can be properly manipulated to contain proteins that are specifically recognized by receptors on target cells, the protein corona can be exploited as the liposome targeting moiety (Figure 1).

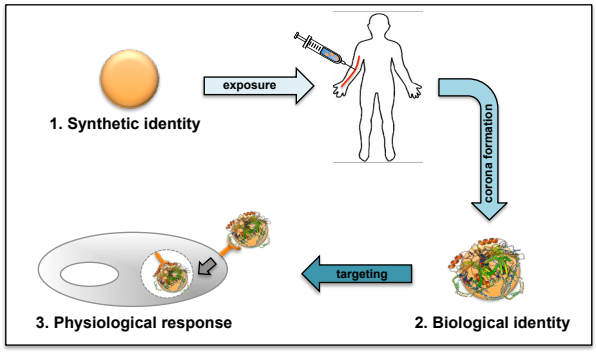

Figure 1. Size, charge, and surface chemistry post-synthesis define the synthetic identity of a liposome. Biological identity is the size, charge and aggregation state of the liposome in the patient's blood, along with the composition of the protein corona. Physiological response is the subsequent interaction of liposomes with receptors of target cells in the body.

In order to properly exploit the protein effect for targeted drug delivery,[21, 22] the ability to design liposomes capable of capturing plasma proteins that are specifically recognized by receptors of target cells is therefore essential. Towards that direction, the first step is a systematic investigation of the identity and properties of the liposomal-protein corona. This will provide important new tools to study liposome-mediated delivery of therapeutic drugs and, importantly, to accurately predict the behavior of liposome formulations in vivo and therefore to manipulate this behavior by liposome design. In order to exploit the liposome-protein corona for targeted drug delivery, the first goal is therefore elucidating the relationship between the lipid composition of liposomal formulations and the protein corona acquired in vivo. Identification of the liposome-corona proteins has been greatly facilitated by recent advances in proteomics and mass spectrometry[5, 23] while recent bio-informatics approaches allow ranking target cells, organs and tissues. Here we have investigated the correlation between liposome lipid composition and the composition of the liposome-protein corona that forms in human plasma (HP). Investigated liposomal formulations were made of those lipid species that are more frequently used for drug delivery purposes such as the cationic lipids 1,2-dioleoyl-3- trimethylammonium-propane (DOTAP) and 3*b*-[N-(*N'*,*N'*-dimethylaminoethane)-carbamoyl]-cholesterol (DC-Chol) and the helper lipids dioleoylphosphatidylethanolamine (DOPE) and cholesterol. To identify and quantify the proteins associated with the corona we have applied high-resolution nanoliquid-cromatography mass spectroscopy (NanoLC-MS/MS). Notably, both non-specific and specific effects contributing to protein adhering to liposomes were identified. The ability to specifically manipulate the liposome-protein corona effect for targeted drug delivery will influence the direction of future research related to the development of liposomal therapeutics.

Experimental

Chemicals and standards

1,2-dioleoyl-3- trimethylammonium-propane (DOTAP), 3*b*-[N-(*N'*,*N'*-dimethylaminoethane)-carbamoyl]-cholesterol (DC-Chol) and dioleoylphosphatidylethanolamine (DOPE) lipids were purchased from Avanti Polar Lipids (Alabaster, AL, USA) and used without further purification. Cholesterol was purchased from Sigma Aldrich (St. Luis, MO, USA). All chemicals were from Sigma Aldrich unless otherwise stated. Organic solvents were from Carlo Erba Reagents (Milan, Italy). The sequencing grade modified trypsin was from Promega (Madison, WI, USA). Ultrapure water (resistivity 18.2 MΩ cm) was obtained by an Arium water purification system (Sartorius, Florence, Italy). Solid phase extraction (SPE) C18 cartridges were BOND ELUT (Varian, Palo Alto, CA, USA).

Human plasma

Human whole blood was obtained by venipuncture of ten healthy volunteers aged 20–40 years at the Department of Experimental Medicine ('Sapienza' University of Rome) according with the institutional bioethics code. After blood collection, K2 EDTA anticoagulant and protease inhibitors cocktail were immediately added to HP. Aliquots were stored at −80 °C in labeled Protein LoBind tubes (Eppendorf, Milan, Italy) to ensure plasma stability until use. When used, aliquots were thawed at 4°C and then left to warm at room temperature.

Cationic liposomes preparation

DOTAP, DOTAP-DOPE, DOTAP-cholesterol, DC-Chol, DC-Chol-DOPE and DC-Chol-cholesterol unilamellar cationic liposomes (CLs) were prepared according to standard protocols by dissolving appropriate amounts of lipids at ϕ = neutral lipid/total lipid (mol/mol)=0.5. Lipid films were hydrated (final lipid concentration 1 mg/mL) with ultrapure water, sonicated with a tip sonicator and stored at 4°C for size and Zeta-potential measurements. For proteomics experiments lipid films were hydrated with a dissolving buffer (Tris–HCl, pH 7.4, 10 mmol/L; NaCl, 150 mmol/L; EDTA, 1 mmol/L) and stored at 4°C.

Size and Zeta-potential experiments

The size and Zeta-potential experiments were made at 37 °C on a Zetasizer Nano ZS90 (Malvern, U.K.) spectrometer equipped with a 5 mW HeNe laser (wavelength λ = 632.8 nm) and a digital logarithmic correlator. By using the CONTIN approach,[24] the normalized intensity autocorrelation functions were analyzed in order to obtain the distribution of the particles diffusion coefficient (D). D is translated into hydrodynamic radius (R_H) through the Stokes-Einstein equation $R_H = K_BT/(6\pi\eta D)$, where K_BT is the thermal energy and η is the solvent viscosity. The same apparatus used for size measurements was employed for zeta potential experiments. This time the mobility *u* was measured by means of the laser

Doppler electrophoresis technique. The mobility *u* was converted into the Zeta-potential through the Smoluchowski relation Zeta-potential = uη/ε, where η and ε are the viscosity and the permittivity of the solvent phase respectively. Results are given as mean ± standard deviation of not less than five replicates.

Synchrotron Small Angle X-ray Scattering

Synchrotron Small Angle X-ray Scattering (SAXS) experiments were carried out at the Austrian SAXS station of the synchrotron light source ELETTRA (Trieste, Italy).[25] SAXS scans were recorded with gas detectors based on the delay line principle spanning the *q*-ranges from q_{min} = 0.005 nm^{-1} to q_{max}= 5 nm^{-1} with a resolution of 5 × 10^{-3} nm^{-1} (fwhm). The angular calibration of the detectors was performed with silver behenate powder (*d*-spacing of 58.38 Å). The data have been properly normalized. Usually exposure times were 100 s. No radiation damage was observed in the SAXS patterns. The sample was held in a 1 mm glass capillary (Hilgenberg, Malsfeld, Germany) and the measurements were executed at 25 °C with a precision of 0.1 °C.

Proteomics experiments

200 µL of liposomes (1 mg/mL) were incubated with 200 µL of human plasma at 37 °C for 1 h. Concentration of liposomes was chosen according to protocols of pre-clinic animal studies. Indeed, to deliver some tenths of micrograms of either drugs or genes, roughly 100 microliters of a liposome solution with a concentration around 1 mg/ml are typically used.[26] This volume is chosen due to the small average total blood volume of a mouse (an adult mouse has a circulating blood volume of about 1.5-2.5 ml) and in virtue of the need to administer twice daily for three/four consecutive days. The liposome-human plasma 1:1 volume ratio was chosen according to previous studies.[13] Typical results after the protein corona has stabilized, spanning biologically relevant plasma concentrations, have shown that starting from 50% plasma concentration, the aggregation state, thickness and composition of the protein corona are pretty stable and resemble those that actually exist in vivo (i.e. at high protein concentration > 80% plasma concentration as, for example, in the blood) with saturation occurring at around 40-80% plasma concentration[27]. Several studies have investigated the time evolution of the protein corona. In recent works, it has been shown that the protein corona form rapidly around nanoparticles (t<30 s) and it does not dramatically evolve in time with typical plateau reached at t=1h.[17-19] This seems to be a relevant incubation time since it resembles the lifetime of many liposomal drugs. After incubation, liposome-protein complexes were centrifuged for 15 min at 14000 rpm. Unbound proteins were removed washing pellets three times with 200 µL of the dissolving buffer. To assure statistical significance of data, nine replicates were performed.

In solution digestion and desalting

The protein pellets were resuspended in 25 µL of a denaturant buffer composed of 8 mol/L urea in 50 mmol/L NH_4HCO_3, and incubated for 1 h at 37 °C. After protein denaturation, 1.25 µL DTT 200 mmol/L in 50 mmol/L NH_4HCO_3 were added to break disulfide bonds and samples were incubated for 1 h at 37 °C. Then 5 µL IAA 200 mmol/L in 50 mmol/L NH_4HCO_3 were added to alkylate thiol groups and samples were left in the dark at room temperature for 1 h. Finally any leftover alkylating reagent was removed by additional 5 µL DTT solution and incubation at 37 °C for 1 h. Then samples were diluted with 50 mmol/L NH_4HCO_3 to reach the final 1mol/L urea concentration and trypsin was added in order to ensure a minimum enzyme-to-substrate ratio of 1:20. Enzymatic digestion was carried out overnight at 37 °C and quenched with trifluoroacetic acid (TFA). Digested samples were desalted using an SPE C18 column (Bond Elut 1CC LRCC18, Varian, Palo Alto, CA, USA) and eluted with 0.5 mL H_2O:ACN (50:50, v/v) solution containing 0.1 % TFA. After lyophilization in a Speed-Vac apparatus (mod. SC 250 Express; Thermo Savant, Holbrook, NY, USA), samples were reconstituted with 0.1% HCOOH solution to obtain a final concentration of 0.32 mg/mL and stored at -80°C until nanoLC-MS/MS analysis. The method of separation is an established method that is commonly followed to separate liposome-protein complexes from unbound proteins.[5, 13, 27] The efficiency of the method has been proven by control experiments showing that, in the absence of liposomes, no pellet forms.

Nanoliquid chromatography tandem mass spectrometry

Tryptic peptides were analyzed by a Dionex Ultimate 3000 (Sunnyvale, CA, USA) nanoLC system connected to the hybrid mass spectrometer LTQ Orbitrap XL (Thermo Fisher Scientific Bremen, Germany), equipped with a nanoelectrospray ion source. 5 µL of peptide mixture were on-line enriched onto a 300 µm i.d. x 5 mm Acclaim PepMap 100 C18 (5 µm particle size, 100 Å pore size) µ-precolumn (Dionex), using a premixed mobile phase H_2O:ACN 98:2 (v/v) containing 0.1% HCOOH, at 10 µL min^{-1} flow-rate. Peptide mixtures were separated by reversed-phase chromatography on in-house manufactured 25 cm long silica micro-column, with a 75 µm i.d and packed with ReproSil-Pur C18-AQ 2.2 µm resin (Dr. Maisch GmbH, Ammerbuch, Germany). Mobile phase was H_2O (A) and ACN (B), both with 0.1% (v/v) HCOOH. After a 5 min isocratic step at 5%, B was linearly increased from 5% to 30% within 130 min and then to 45% in 10 min. After that, B was increased to 80% within 10 min and kept constant for 10 min. Then, B was decreased to 5% within 1 min and kept constant for the following 30 min to rinse the column. Separation was made at a flow rate of 300 nL min^{-1}. MS spectra were collected over the 400-1800 *m/z* range at 60000 resolution, operating in the data dependent mode and TOP5 mode, i.e. MS/MS spectra were collected for the five most intense ions with a charge state greater than 1, using a dynamic exclusion of 60 s. CID was performed with normalized collision energy at 35 V. All samples were analyzed in triplicate to assess the variation due

to the experimental procedure and to increase the number of identified proteins.

Data analysis and protein validation

Xcalibur (v.2.07, ThermoFisher Scientific) raw data files were submitted to Proteome Discover (1.2 version, Thermo Scientific) for database search using Mascot (version 2.3.2 Matrix Science). Data were searched against SwissProt database (57.15 version, 20266 sequences) using the decoy search option of Mascot. Enzymatic digestion with trypsin was selected, along with maximum 2 missed cleavages, peptide charges +2 and +3, 10 ppm precursor mass tolerance and 0.8 Da fragment mass tolerance; acetylation (N-term), oxidation (M) and deamidation (N, Q) were used as dynamic modifications; carbamidomethylation (C) was used as static modification. The Scaffold software (version 3.1.2, Proteome Software Inc.)[28] was used to validate MS/MS-based peptide and protein identifications and for label-free relative quantitation based on spectral counting. The peptide and protein probabilities were set to minimum 95% and 99%, respectively, with at least two unique peptides for each identification. For protein quantitative analysis, Scaffold software allows the normalization of the spectral countings (normalized spectral countings, NSCs) and offers various statistical tests to identify significant abundance differences in two or more categories. The mean value of NSCs from nine experimental replicates was calculated for each protein and then normalized to the protein molecular weight (MWNSC). The relative protein quantity was obtained by applying the following equation:[13]

$$\mathrm{MWNSC}_k = \frac{(\mathrm{NSC}/\mathrm{MW})_k}{\sum_{i=1}^{N}(\mathrm{NSC}/\mathrm{MW})_i} \times 100 \qquad (1)$$

where MWNSC_k is the percentage molecular weight normalized NSC for protein k, and MW is the molecular weight in kDa for protein k. This correction takes into account the protein size and evaluates the real contribution of each protein. According to literature[13], MWNSC_k is assumed as a good estimation of the relative protein abundance (RPA) in the corona.

Results and Discussion

Size and zeta-potential

First, size and zeta-potential of DOTAP, DOTAP–DOPE, DOTAP–cholesterol, DC-Chol, DC-Chol–DOPE and DC-Chol–cholesterol supra-molecular assemblies were measured (Table 1). They were found to be small-size aggregates with mean diameter between 80 and 120 nm. Synthesized CLs were positively charged with zeta-potential ranging from 50.5 mV (DOTAP–cholesterol) to 59.6 mV (DC-Chol), with the other four formulations exhibiting intermediate values. After 1h incubation with HP, size of CL–HP complexes was larger than that of CLs (Table 1). Comparing the DLS size distributions of liposomes with those of liposome-protein complexes (Figure S1 of Electronic Supplementary Material), we conclude that liposome aggregation occurred. This result is in good agreement with previously reported findings.[10] As result of protein corona formation, zeta-potential of CL-HP complexes reversed to slightly negative values. Drop in the surface charge from positive to slightly negative values is most likely to result in liposome clustering.

	Buffer		HP	
	Size (nm)	Zeta-potential (mV)	Size (nm)	Zeta-potential (mV)
DOTAP	78.8±2.2	55.7±1.8	156.5±4.5	-1.5±0.5
DOTAP-DOPE	90.8±1.1	51.2±1.8	178.1±3.7	-2.1±0.8
DOTAP-cholesterol	83.5±1.3	50.5±1.3	187.4±7.8	-2.4±0.7
DC-Chol	99.6±1.1	59.2±1.7	220±4	-10.6±0.3
DC-Chol-DOPE	119.2±0.7	56.3±1.3	250±2	-11.4±0.8
DC-Chol-cholesterol	85.6±2.1	55.6±1.1	210±6	-11.2±0.5

Table 1. Size and zeta-potential of DOTAP, DOTAP-DOPE, DOTAP-cholesterol, DC-Chol, DC-Chol-DOPE and DC-Chol-cholesterol cationic liposomes in buffer and after 1h incubation with human plasma.

Nanostructure

To support conclusions of DLS experiments, synchrotron small angle X-ray scattering (SAXS) was employed. Panels A and B of Figure 2 show that lipid vesicles exhibited only pure diffuse scattering, which is typical of uncorrelated bilayers such as unilamellar liposomes.

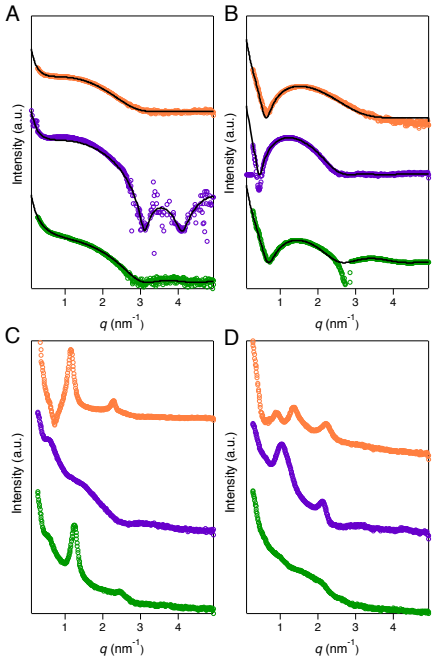

Figure 2. Synchrotron SAXS patterns of: (A) DOTAP (green circles), DOTAP-DOPE (violet circles) and DOTAP-cholesterol (orange circles) cationic liposomes; (B) DC-Chol (green circles), DC-Chol-DOPE (violet circles) and DC-Chol-cholesterol (orange circles) cationic liposomes. Solid lines are the best fits to the data using Eq. 2. (C) DOTAP (green circles), DOTAP-DOPE (violet circles) and DOTAP-cholesterol (orange circles) cationic liposomes after 1 h incubation with human plasma (HP); (D) DC-Chol (green circles), DC-Chol-DOPE (violet circles) and DC-Chol-cholesterol (orange circles) cationic liposomes after 1 h incubation with human plasma (HP).

The scattered intensity was therefore fitted with the easiest of the representative bilayer models in which the electron density profile is given by the superposition of a negative

Gaussian at the center of the lipid bilayer accounting for the hydrophobic chains plus two positive Gaussians representing the lipid headgroups: [29]

$$I(q) = 2\pi \frac{[2\sigma_H \exp(-\sigma_H^2 q^2/2)\cos(qz_H) - \sigma_C \rho \exp(-\sigma_C^2 q^2/2)]^2}{q^2} \quad (2)$$

where σ_H is the half width at half maximum of the Gaussian that represents the polar region, z_H is the distance of the lipid headgroup from the bilayer center, ρ is the ratio between the methyl terminus electron density amplitude and the headgroup, σ_C is the standard deviation of the Gaussian at the center of the bilayer accounting for the hydrocarbon chains, and the $1/q^2$ term is the Lorentz correction factor for isotropic scatterers.

	d_B(nm)
DOTAP	3.51±0.05
DOTAP-DOPE	4.00±0.06
DOTAP-cholesterol	3.95±0.05
DC-Chol	3.72±0.04
DC-Chol-DOPE	4.40±0.03
DC-Chol-cholesterol	3.70±0.06

Table 2. Liposome bilayer thickness, d_B, of cationic liposomes calculated by using Eq. 2.

The best fitting model functions using Eq. (2) are also shown in Figure 2. Among the six investigated formulations, those containing DOTAP are indubitably liposomes. DC-Chol-DOPE assemblies are liposomes as well. On the other side, the exact nature of DC-Chol and DC-Chol-cholesterol aggregates has been marginally addressed so far. As a first step, we tried to fit the synchrotron SAXS profiles of DC-Chol and DC-Chol-cholesterol using many different models for the oscillating part of the form factor such as spherical micelle, fuzzy sphere and cylindrical micelle. None of them could match the experimental SAXS profiles, and they were then discarded. On the other side, as Figure 2 panel B clearly shows, the synchrotron SAXS profiles of both DC-Chol and DC-Chol-cholesterol were well fitted by Eq. 2. Since the oscillating part of the form factor contains information about the internal electron density distribution, the good agreement between the experimental SAXS intensity and the theoretical value predicted by Eq. 2 seems to suggest that both DC-Chol and DC-Chol-cholesterol are bilayers on the nanometer scale. Investigating the power law of the form factor at low q allows clarifying the aggregate shape. Such analysis allowed us to conclude that DC-Chol-cholesterol assemblies are liposomes (Figure S2 of Electronic Supplementary Material). This result is in very good agreement with recent findings reported in the literature.[30] On the other side, SAXS results clarified that the structure of DC-Chol is made of globular aggregates whose surface has fractal features (power law slightly different from the Porod q^{-4} behavior) made of a planar substructure. In previous investigations,[11, 31-33] we have shown that lipid composition is the main factor shaping the protein corona. Since the goal of this work was to investigate the existence of a correlation between lipid species and classes of plasma proteins, the fact that DC-Chol aggregates are not liposomes does not affect the conclusions of the work. From the fitting procedure, we could calculate the liposome bilayer thickness, d_B, (Table 2). Synchrotron SAXS patterns of liposome–HP complexes are shown in Figure 2 (panels, C and D). While the intensity distribution of CLs in the absence of the protein corona was dominated by the bilayer form factor (Figure 2), the SAXS patterns of CL–HP complexes exhibited quasi-Bragg peaks due to the intra-particle structure factor. Even though a detailed structural analysis goes beyond the scope of this work, our synchrotron SAXS findings corroborate DLS results giving demonstration that, following incubation with HP, liposome aggregation occurs.

Braford assays results

Figure 3 shows the amount of proteins absorbed onto the surface of CLs after 1 h of incubation with HP. Bradford assay results demonstrate that protein binding is slightly dependent on the lipid species. In general, DOTAP-containing CLS seemed to be less protein enriched than their DC-Chol-containing counterpart.

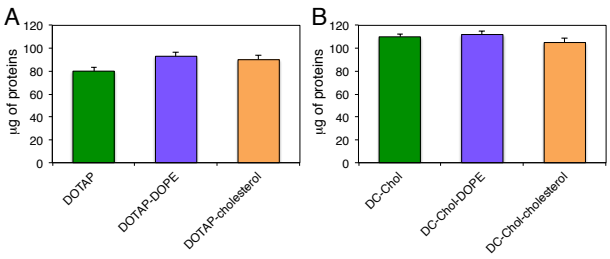

Figure 3. Micrograms of proteins bound to: (A) DOTAP, DOTAP-DOPE, and DOTAP-cholesterol cationic liposomes and (B) DC-Chol, DC-Chol-DOPE and DC-Chol-cholesterol cationic liposomes after 1 h incubation with human plasma (HP) as determined by Bradford assay. Results are given as means ± standard deviation of three independent replicates.

Protein identification

Supplementary Table S1 summarizes the identification of plasma proteins adhering to the six liposomal formulations after 1 h incubation with HP. As a first step toward elucidating the effect of lipid composition on the protein corona, the number of unique and common can be evaluated. This is usually shown by Venn diagrams as those reported in Figure 4. As evident, Venn diagrams provide a clear overview of the relationship existing between the proteins identified in the coronas. Considering DOTAP-containing CLs (Figure 4, panel A), we observe that only 96 of 318 identified proteins (30%) are in common. The coronas of both DOTAP–DOPE (209 identified proteins) and DOTAP–cholesterol (248 identified proteins) CLs were much more enriched than that of plain DOTAP liposomes (135 identified proteins). This outcome demonstrates that the substituting cationic with neutral molecules, being either DOPE or cholesterol, drastically affects the composition of the protein corona. In Figure 4, panel B the Venn diagram of DC-Chol-containing CLs is shown. In this case, 100 of 201 identified proteins (50%) were common between formulations. When half of DC-Chol molecules were substituted by DOPE, 34 new proteins bound. In addition, 67 proteins found on both DC-Chol and DC-Chol-cholesterol CLs were

not identified in DC-Chol-DOPE CLs. Thus, substitution of half of the cholesterol-like molecules by DOPE impairs the binding of roughly 40% of identified proteins (67 on 167). This observation supports the idea that the nanoparticle surface chemistry is a major factor that shapes the protein corona. The number of unique proteins of DC-Chol-DOPE CLs (34) is very similar to its counterpart identified in DOTAP–DOPE CLs (36). On the other side, cholesterol did not change the proteome of DC-Chol assemblies. Collectively, results of Figure 4 seem to suggest that, while DOPE binds new proteins independently on the cationic lipid, cholesterol does not. When mixed with DOTAP, cholesterol likely changes the surface properties of CLs leading to adsorption of 147 new proteins (77 of which are unique), while it does not affect the binding ability of DC-Chol supramolecular assemblies (no unique proteins identified). DC-Chol is a cationic molecule with a d tertiary ammino group covalently bound to the cholesterol moiety. Thus, it is conceivable to suppose that packing of cholesterol between DC-Chol molecules is energetically favorable with the result that cholesterol inclusion produce minor changes, if any, to the lipid surface.

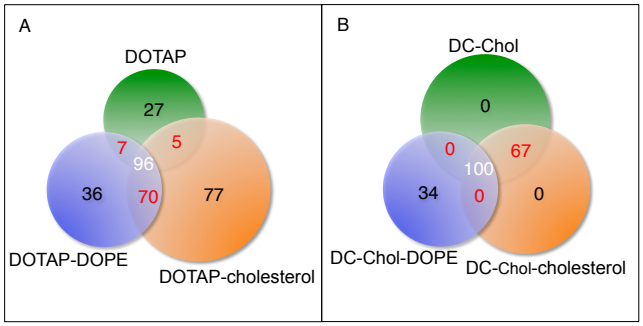

Figure 4. Venn diagram reporting the number of proteins identified in the DOTAP- (A) and DC-Chol- (B) containing cationic liposomes.

Protein quantification

The relative protein abundance (RPA) of all the proteins identified in the coronas of the six lipid formulations was calculated using Eq. 1 (see Experimental section). The most abundant plasma proteins adhering to DOTAP- and DC-Chol-containing CLs are reported in Table 3 and Table 4 respectively. For clarity, we considered classes of proteins and single proteins with RPA≥1% in at least one corona. Apolipoproteins, immunoglobulins (Igs) and complement proteins were the most enriched classes of proteins, while fibrinogen, prothrombin, serum albumin, vitamin-k and vitronectin were the most abundant single proteins. With this threshold (RPA≥1%), we could take into account the largest part of the protein corona ranging from 51.4% (DOTAP–cholesterol) to 65.3% (DOTAP) of the total protein content. To elucidate the role played by each lipid species on the corona formation, we calculated the ratio between the RPAs of every single protein (or class of protein) for each couple of formulations, R. As a first step, we used R to compare the coronas of DOTAP–DOPE and DOTAP–cholesterol CLs with that of plain DOTAP ones (Figure 5, panels A and B respectively).

	RPA(%)		
	DOTAP	DOTAP-DOPE	DOTAP-cholesterol
Apolipoprotein	13.7	29.6	17.6
Vitronectin	13.3	8.9	2.7
Fibrinogen	10.8	2.9	5.9
Ig	6.6	6.2	11.1
Prothrombin	5.1	1.1	0.8
Complement	4.8	2.5	7.4
Serum Albumin	4.5	8.6	4.1
Vitamin-k	4.2	0.7	0.9
Clusterin	2.3	3.7	0.9

Table 3. Relative protein abundance of the most abundant plasma proteins adhering to DOTAP-containing CLs after 1h incubation with HP as identified by nanoLC-MS/MS.

	RPA(%)		
	DC-Chol	DC-Chol-DOPE	DC-Chol-cholesterol
Ig	16.8	9.9	16.8
Complement	9.4	5.2	7.2
Apolipoprotein	8.9	25.2	10.9
Fibrinogen	7.7	4.6	8.4
Vitamin-k	6.1	0.4	3.9
Serum Albumin	4.7	5.5	4.6
Prothrombin	4.1	0.7	3
Vitronectin	2.9	1.8	2.5
Clusterin	0.7	1.2	1.6

Table 4. Relative protein abundance of the most abundant plasma proteins adhering to DC-Chol-containing CLs after 1h incubation with HP as identified by nanoLC-MS/MS.

Remarkably, fibrinogen, prothrombin, vitamin K, and vitronectin coalesced on the same region of R (R≤0.5). This result suggests that substituting cationic DOTAP with neutral lipids, being indifferently DOPE or cholesterol, decrease the affinity of those proteins for the vesicle surface. Since fibrinogen, prothrombin, vitamin K, and vitronectin are negatively charged proteins at physiological pH, this finding is most likely to indicate that substituting DOTAP molecules with neutral lipids decreases the net charge of the lipid vesicle making it less attractive for the electrostatic binding of anionic plasma proteins. This effect is likely due to the molecular structure of DOTAP, a double chain quaternary ammonium cationic surfactant that is permanently charged, independent of the pH of the solution. As Table 3 shows, vitronectin was found to be the most enriched single protein in the corona of DOTAP liposomes (RPA ≈ 13.3%). Vitronectin is a 75 kDa glycoprotein consisting of 459 amino acid residues. It contains an RGD (45-47) sequence, which is a binding site for membrane-bound integrins, e.g., the vitronectin receptor ($\alpha_v\beta_3$ integrins). In a recent work,[34] we have shown that a vitronectin-enriched protein corona can be exploited to target highly metastatic MDA-MB-435S cells that express high levels of the vitronectin receptor $\alpha_v\beta_3$ integrin. More in detail, fluorescence confocal microscopy experiments proved that bare DOTAP vesicles do not bind to the vitronectin receptor before being internalized, while, in the presence of a vitronectin-enriched protein corona, lipid vesicles are internalized by an integrin-mediated mechanism. This study provided the first proof-of-concept about the exploitation of the protein corona for targeted delivery in vitro. Figure 5, panel A clearly shows that DOPE promotes the adsorption of typical dysopsonins such as apolipoproteins and serum albumin (R > 1).

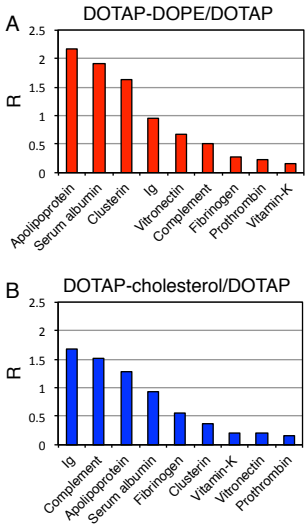

Figure 5. Relative ratio, R, of the relative protein abundance (RPA) of the most abundant proteins found in the corona of (A) DOTAP-DOPE and plain DOTAP cationic liposomes and (B) DOTAP-cholesterol and plain DOTAP cationic liposomes. RPA was calculated by Eq. 1.

The Apos enrichment may affect the interaction between liposomes and cells, as lipoprotein complexes play a key role in the cellular processes of cholesterol metabolism. Several receptors for Apo complexes exist on the cell surfaces. For instance, Apolipoprotein B (ApoB), apolipoprotein E (ApoE) and ApoA enhance the uptake of liposomes by hepatocytes.[35, 36] ApoE can also promote interaction with low-density lipoprotein (LDL) receptors, resulting in transport across the blood–brain barrier.[13] Apolipoprotein A-I (ApoA-I)-bound to cationic liposomes targeted siRNA delivery into mouse hepatocytes expressing Hepatitis C virus proteins and inhibited their expression efficiently.[37] Recently, Kim et al.[38] have developed a nanoparticle composed of DOTAP-DOPE CLs enriched with ApoA-I enabled targeted delivery of drugs to the lung tumors. In recent publications,[17, 20] our team showed that an apolipoprotein-enriched protein corona can be exploited to target PC3 and DU145 prostate cancer cells that expressing high levels of scavenger receptor class B type 1 receptor. These studies supported the emerging idea that the liposome-protein corona can be manipulated to target cancer cells. On the other side, cholesterol seems to induce the preferential binding of opsonins such as immunoglobulins (Ig) and complement proteins (R > 1; Figure 5, panel B). This result is quite surprising considering that cholesterol is a main component of approved liposomal anticancer therapeutics, while DOPE is not. In marketed liposomal formulations incorporation of cholesterol was shown to 'tighten' fluid bilayers and reduce the leakage of contents from liposomes.

Our results seem to suggest that a solid phase bilayer with reduced cholesterol content might be a good compromise to promote drug retention and to reduce the binding of proteins that activate the complement system. Remarkably, when we compared the coronas of DC-Chol-DOPE and DC-Chol-cholesterol CLs with that of DC-Chol aggregates by R, comparable results were achieved (Figure 6, panels A and B respectively). The effect of cationic charge found in DOTAP-containing CLs was observed in DC-Chol-containing CLs as well. This is due to the chemical structure of DC-Chol that has a positively charged tertiary ammino group attached to the cholesterol moiety via a carbamoyl bond. However, the equilibrium composition of the corona seems to be controlled by interactions other than electrostatics. Indeed, the protein adsorption profiles of DOTAP and DC-Chol were found to be quite different from each other. While DOTAP induces the preferential adsorption of vitronectin, DC-Chol promotes the binding of Ig and complement proteins (Figure S3 of Electronic Supplementary Material).

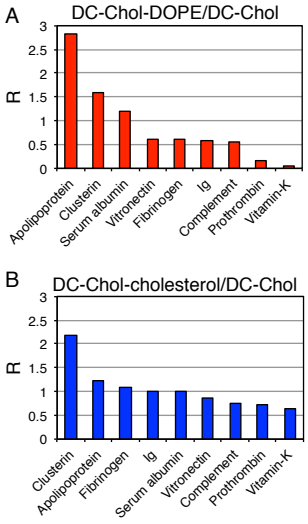

Figure 6. Relative ratio, R, of the relative protein abundance (RPA) of the most abundant proteins found in the corona of (A) DC-Chol-DOPE and plain DC-Chol cationic liposomes and (B) DC-Chol-cholesterol and plain DC-Chol cationic liposomes. RPA was calculated by Eq. 1.

Furthermore, one more consideration regarding neutral lipids can be made. We notice that, when mixed with cationic lipids, DOPE modifies the protein adsorption profiles of DOTAP and DC-Chol similarly, whereas the effect of cholesterol is somewhat more complex. When mixed with DOTAP, cholesterol strongly reduces the affinity of the lipid surface for vitronectin and vitamin-k and promotes binding of Igs and complement proteins. On the other side, in mixture with DC-Chol, cholesterol has a minor effect, if any, in the protein profile of plain DC-Cholesterol aggregates. This confirms the results of Figure 4 showing that DC-Chol and DC-Chol-cholesterol CLs bind exactly the same proteins (i.e. no unique proteins were found). A further comment on the differences between DOPE and cholesterol is mandatory. In previous investigations, we have shown that membrane charge density is a key factor shaping the protein corona.[32] Cholesterol tightens the fluid lipids packing possibly affecting the liposome surface charge intensity. On the other side, we found that DOPE and cholesterol had the same effect on zeta-potential of

cationic membranes (Table 1). Nonetheless, cholesterol can affect the fluid lipids packing and greatly compromises its spacing effect in reducing the membrane area.[39] This reduction could affect the protein adsorption profile. In addition, cholesterol may also promote the formation of domain structure,[40] which, in turn, may induce differences in the protein adsorption profile.

Conclusions

In summary, we employed high-resolution NanoLC-MS/MS to elucidate general principles regulating the bio-nano-interactions between liposomes and HP proteins. In summary, our findings have provided the following body of evidence: i) non-specific interactions, which contribute to protein bio-conjugation, are mainly electrostatic. At physiological pH fibrinogen, prothrombin, vitamin K, and vitronectin bind to cationic liposomes due to their positive charge; ii) plasma proteins bind specifically to functional chemical groups onto the lipid surface: DOTAP specially binds apolipoproteins and vitronectin; DOPE promotes the adsorption of apolipoproteins and serum albumin; both DC-Chol and cholesterol seems to induce the preferential binding of opsonins such as immunoglobulins and complement proteins; iii) the affinity of each lipid species for plasma proteins is affected by the co-presence of other species in the lipid bilayer. Evidently, all these observations should be carefully considered to design cationic lipid nanoparticles for drug delivery both in vitro (transfection in serum media) and in vivo. The ability to specifically manipulate the liposome-protein corona will influence the direction of future research related to the development of liposomal therapeutics. It will allow for the classification of such therapeutics in terms of their corona composition, as this mediates their interaction with the cellular machinery. Manipulation will be affected by factors other than the physicochemical properties of liposomes. A critical factor affecting the composition of the liposome-protein corona might be temperature [16]. Even if it has received less consideration so far, temperature can control the degree of protein coverage and the composition of the corona. This is a point of great general interest as the human body temperature can range from 35.8 to 37.2 °C, is different for any part of the body and can even rise to 41 °C in the case of inflammatory states and fever. Nonetheless, humans with specific diseases may have different levels of plasma proteins in the blood resulting in highly specific protein coronas. Based on these results, Mahmoudi and coworkers introduced the concept of "personalized protein corona" (PPC) as a determinant factor for clinical and biological applications [41]. We have supported the PPC concept in a recent work, where we compared size and zeta-potential of liposomes after incubation of human plasma collected from healthy volunteers and histologically proven pancreatic cancer patients with a statistically significant reduction in the level of clinically relevant proteins were enrolled [42]. At present, a detailed time resolved description of the evolving interactions as nanoparticles in general and liposome in particular are uptaken and trafficked within the cellular environment is lacking. Recently reported results show that major fraction of the original corona is well maintained as nanoparticles are trafficked through the cells.[43] Full understanding of what happens to the protein corona within organelles containing the nanoparticles is mandatory for the emerging arena of nanoparticle-cell interactions to advance.

Notes and references

[a]Department of Molecular Medicine, 'Sapienza' University of Rome, Viale Regina Elena 291, 00161 Rome (Italy).
[b]Department of Cheimistry, 'Sapienza' University of Rome, P.le Aldo Moro 5, 00185 Rome (Italy).
[c]Institute of inorganic Chemistry, Graz University of Technology, Stremayerg 6/IV, 8010 Graz, Austria.
*E-mail: giulio.caracciolo@uniroma1.it

Electronic Supplementary Information (ESI) available: Figure S1. Comparison between the size distributions of DC-Chol-DOPE cationic liposomes and DC-Chol-DOPE-human plasma complexes as detected by dynamic light scattering. Table S1. The full list of all the plasma proteins adhering on the six liposomal formulations after 1 h incubation with HP as identified by NanoLC-MS/MS. Figure S2. Figure S3. Relative protein abundance of the most abundant proteins found in the corona of DOTAP and DC-Chol are compared by their relative ratio, R. See DOI: 10.1039/b000000x/

1. Y. Fan and Q. Zhang, *Asian Journal of Pharmaceutical Sciences*, 2013, 8, 81-87.
2. D. d. S. Ferreira, S. C. d. A. Lopes, M. S. Franco and M. C. Oliveira, *Therapeutic delivery*, 2013, 4, 1099-1123.
3. R. Wang, P. S. Billone and W. M. Mullett, *Journal of Nanomaterials*, 2013, 2013, 1.
4. Y. C. Barenholz, *Journal of controlled release*, 2012, 160, 117-134.
5. T. Cedervall, I. Lynch, S. Lindman, T. Berggård, E. Thulin, H. Nilsson, K. A. Dawson and S. Linse, *Proceedings of the National Academy of Sciences*, 2007, 104, 2050-2055.
6. M. Lundqvist, J. Stigler, G. Elia, I. Lynch, T. Cedervall and K. A. Dawson, *Proceedings of the National Academy of Sciences*, 2008, 105, 14265-14270.
7. I. Lynch and K. A. Dawson, *Nano Today*, 2008, 3, 40-47.
8. P. Aggarwal, J. B. Hall, C. B. McLeland, M. A. Dobrovolskaia and S. E. McNeil, *Advanced Drug Delivery Reviews*, 2009, 61, 428-437.
9. I. Lynch, A. Salvati and K. A. Dawson, *Nature nanotechnology*, 2009, 4, 546-547.
10. D. Walczyk, F. B. Bombelli, M. P. Monopoli, I. Lynch and K. A. Dawson, *Journal of the American Chemical Society*, 2010, 132, 5761-5768.
11. G. Caracciolo, D. Pozzi, A. L. Capriotti, C. Cavaliere, P. Foglia, H. Amenitsch and A. Laganà, *Langmuir*, 2011, 27, 15048-15053.
12. M. Lundqvist, J. Stigler, T. Cedervall, T. Berggård, M. B. Flanagan, I. Lynch, G. Elia and K. Dawson, *ACS nano*, 2011, 5, 7503-7509.

13. M. P. Monopoli, D. Walczyk, A. Campbell, G. Elia, I. Lynch, F. Baldelli Bombelli and K. A. Dawson, *Journal of the American Chemical Society*, 2011, 133, 2525-2534.
14. S. Tenzer, D. Docter, S. Rosfa, A. Wlodarski, J. r. Kuharev, A. Rekik, S. K. Knauer, C. Bantz, T. Nawroth and C. Bier, *ACS nano*, 2011, 5, 7155-7167.
15. M. Mahmoudi, S. N. Saeedi-Eslami, M. A. Shokrgozar, K. Azadmanesh, M. Hassanlou, H. R. Kalhor, C. Burtea, B. Rothen-Rutishauser, S. Laurent, S. Sheibani and H. Vali, *Nanoscale*, 2012, 4, 5461-5468.
16. M. Mahmoudi, A. M. Abdelmonem, S. Behzadi, J. H. Clement, S. Dutz, M. R. Ejtehadi, R. Hartmann, K. Kantner, U. Linne and P. Maffre, *ACS nano*, 2013, 7, 6555-6562.
17. A. L. Barrán-Berdón, D. Pozzi, G. Caracciolo, A. L. Capriotti, G. Caruso, C. Cavaliere, A. Riccioli, S. Palchetti and A. Laganaì, *Langmuir*, 2013, 29, 6485-6494.
18. M. Lundqvist, *Nature nanotechnology*, 2013, 8, 701-702.
19. S. Tenzer, D. Docter, J. Kuharev, A. Musyanovych, V. Fetz, R. Hecht, F. Schlenk, D. Fischer, K. Kiouptsi and C. Reinhardt, *Nature nanotechnology*, 2013, 8, 772-781.
20. D. Pozzi, V. Colapicchioni, G. Caracciolo, S. Piovesana, A. L. Capriotti, S. Palchetti, S. De Grossi, A. Riccioli, H. Amenitsch and A. Laganà, *Nanoscale*, 2014.
21. G. Caracciolo, *Bioinspired, Biomimetic and Nanobiomaterials*, 2012, 2, 54-57.
22. E. Mahon, A. Salvati, F. Baldelli Bombelli, I. Lynch and K. A. Dawson, *Journal of Controlled Release*, 2012, 161, 164-174.
23. Z. W. Lai, Y. Yan, F. Caruso and E. C. Nice, *ACS nano*, 2012, 6, 10438-10448.
24. S. W. Provencher, *Computer Physics Communications*, 1982, 27, 229-242.
25. H. Amenitsch, M. Rappolt, M. Kriechbaum, H. Mio, P. Laggner and S. Bernstorff, *Journal of synchrotron radiation*, 1998, 5, 506-508.
26. D. Simberg, S. Weisman, Y. Talmon, A. Faerman, T. Shoshani and Y. Barenholz, *Journal of Biological Chemistry*, 2003, 278, 39858-39865.
27. T. Cedervall, I. Lynch, M. Foy, T. Berggård, S. C. Donnelly, G. Cagney, S. Linse and K. A. Dawson, *Angewandte Chemie International Edition*, 2007, 46, 5754-5756.
28. B. C. Searle, *Proteomics*, 2010, 10, 1265-1269.
29. G. Pabst, R. Koschuch, B. Pozo-Navas, M. Rappolt, K. Lohner and P. Laggner, *Journal of applied crystallography*, 2003, 36, 1378-1388.
30. S.-y. Yang, Y. Zheng, J.-y. Chen, Q.-y. Zhang, D. Zhao, D.-e. Han and X.-j. Chen, *Colloids and Surfaces B: Biointerfaces*, 2013, 101, 6-13.
31. A. L. Capriotti, G. Caracciolo, G. Caruso, P. Foglia, D. Pozzi, R. Samperi and A. Lagan, *Analytical Biochemistry*, 2011, 419, 180-189.
32. G. Caracciolo, D. Pozzi, S. Candeloro De Sanctis, A. Laura Capriotti, G. Caruso, R. Samperi and A. Laganà, *Applied Physics Letters*, 2011, 99.
33. A. L. Capriotti, G. Caracciolo, C. Cavaliere, P. Foglia, D. Pozzi, R. Samperi and A. Laganà, *Journal of Proteomics*, 2012, 75, 1924-1932.
34. G. Caracciolo, F. Cardarelli, D. Pozzi, F. Salomone, G. Maccari, G. Bardi, A. L. Capriotti, C. Cavaliere, M. Papi and A. Laganà, *ACS applied materials & interfaces*, 2013, 5, 13171-13179.
35. K. Williams, V. Werth and J. Wolff, *Perspectives in biology and medicine*, 1984, 27, 417.
36. C. L. Bisgaier, M. V. Siebenkas and K. J. Williams, *Journal of Biological Chemistry*, 1989, 264, 862-866.
37. S. I. Kim, D. Shin, H. Lee, B.-Y. Ahn, Y. Yoon and M. Kim, *Journal of hepatology*, 2009, 50, 479-488.
38. S. K. Kim, M. B. Foote and L. Huang, *Biomaterials*, 2012, 33, 3959-3966.
39. C. Chen and C. P. Tripp, *Biochimica et Biophysica Acta (BBA)-Biomembranes*, 2008, 1778, 2266-2272.
40. E. E. Berring, K. Borrenpohl, S. J. Fliesler and A. B. Serfis, *Chemistry and physics of lipids*, 2005, 136, 1-12.
41. M. J. Hajipour, S. Laurent, A. Aghaie, F. Rezaee and M. Mahmoudi, *Biomaterials Science*, 2014, 2, 1210-1221.
42. G. Caracciolo, D. Caputo, D. Pozzi, V. Colapicchioni and R. Coppola, *Colloids and Surfaces B: Biointerfaces*, DOI: http://dx.doi.org/10.1016/j.colsurfb.2014.10.008.
43. F. Bertoli, G. L. Davies, M. P. Monopoli, M. Moloney, Y. K. Gun'ko, A. Salvati and K. A. Dawson, *Small*, 2014.